# Fault slip and seismic moment of the 1700 Cascadia earthquake inferred from Japanese tsunami descriptions

Kenji Satake
Active Fault Research Center, Geological Survey of Japan/AIST, Tsukuba, Japan

Kelin Wang
Pacific Geoscience Centre, Geological Survey of Canada, Sidney, British Columbia, Canada

Brian F. Atwater
United States Geological Survey at Department of Earth and Space Sciences, University of Washington, Seattle, Washington, USA

Received 27 March 2003; revised 6 July 2003; accepted 23 July 2003; published 20 November 2003.

[1] The 1700 Cascadia earthquake attained moment magnitude 9 according to new estimates based on effects of its tsunami in Japan, computed coseismic seafloor deformation for hypothetical ruptures in Cascadia, and tsunami modeling in the Pacific Ocean. Reports of damage and flooding show that the 1700 Cascadia tsunami reached 1–5 m heights at seven shoreline sites in Japan. Three sets of estimated heights express uncertainty about location and depth of reported flooding, landward decline in tsunami heights from shorelines, and post-1700 land-level changes. We compare each set with tsunami heights computed from six Cascadia sources. Each source is vertical seafloor displacement calculated with a three-dimensional elastic dislocation model. For three sources the rupture extends the 1100 km length of the subduction zone and differs in width and shallow dip; for the other sources, ruptures of ordinary width extend 360–670 km. To compute tsunami waveforms, we use a linear long-wave approximation with a finite difference method, and we employ modern bathymetry with nearshore grid spacing as small as 0.4 km. The various combinations of Japanese tsunami heights and Cascadia sources give seismic moment of $1–9 \times 10^{22}$ N m, equivalent to moment magnitude 8.7–9.2. This range excludes several unquantified uncertainties. The most likely earthquake, of moment magnitude 9.0, has 19 m of coseismic slip on an offshore, full-slip zone 1100 km long with linearly decreasing slip on a downdip partial-slip zone. The shorter rupture models require up to 40 m offshore slip and predict land-level changes inconsistent with coastal paleoseismological evidence. *INDEX TERMS:* 1242 Geodesy and Gravity: Seismic deformations (7205); 4564 Oceanography: Physical: Tsunamis and storm surges; 7215 Seismology: Earthquake parameters; 7221 Seismology: Paleoseismology; 8150 Tectonophysics: Plate boundary—general (3040); *KEYWORDS:* Cascadia, Japan, subduction zone, earthquake, tsunami

**Citation:** Satake, K., K. Wang, and B. F. Atwater, Fault slip and seismic moment of the 1700 Cascadia earthquake inferred from Japanese tsunami descriptions, *J. Geophys. Res.*, *108*(B11), 2535, doi:10.1029/2003JB002521, 2003.

## 1. Introduction

[2] The Cascadia subduction zone, which extends 1100 km along the Pacific coast of North America (Figure 1), produces infrequent earthquakes of moment magnitude ($M_w$) 8 or larger. The possibility of these great earthquakes was first inferred from geodesy [*Savage et al.*, 1981] and from geophysical and tectonic similarities with other subduction zones [*Heaton and Kanamori*, 1984]. The past occurrence of great Cascadia earthquakes, at intervals averaging about 500 years, was then shown by paleoseismology [*Clague*, 1997].


0148-0227/03/2003JB002521$09.00

[3] The most recent of Cascadia's great earthquakes occurred in 1700 A.D. Evidence for this date comes from North America and Japan. In North America, radiocarbon-dated evidence for coseismic subsidence and tsunami shows that at least 900 km of the Cascadia subduction zone ruptured after 1660; the most precise of the radiocarbon ages, from estuaries in Washington and California, limit the time of rupture to 1690–1720 [*Nelson et al.*, 1995]. Tree ring dating further limits the rupture time off southern Washington to the months between August 1699 and May 1700 [*Jacoby et al.*, 1997; *Yamaguchi et al.*, 1997]. In Japan, which has a documented history of trans-Pacific tsunamis as early as 1586 [*Watanabe*, 1998], a widespread tsunami of remote origin struck Honshu's Pacific coast in January 1700 [*Satake et al.*, 1996; *Tsuji et al.*, 1998]. *Satake*

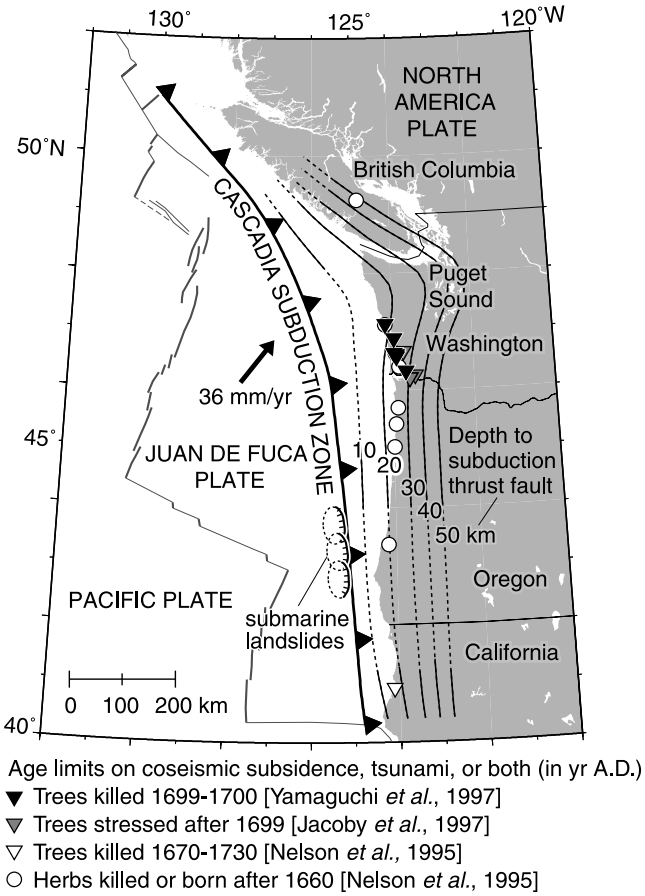


**Figure 1.** Tectonic setting of the Cascadia subduction zone, showing depth contours of subduction thrust fault and barbed line indicating the seaward edge [*Flück et al.*, 1997], best dated evidence for an earthquake about 300 years ago, and large submarine landslides of Pleistocene age [*Goldfinger et al.*, 2000].

*et al.* [1996] showed that the 1700 tsunami corresponds to no documented earthquake in Kamchatka, Aleutians, or South America. They concluded that the tsunami originated at the Cascadia subduction zone; and from its date and time in Japan, they inferred that the tsunami originated about 2100 Pacific Standard Time on 26 January 1700.

[4] In addition to giving this exact time for a great Cascadia earthquake, old documents in Japan provide decisive clues about the earthquake's size. Geological dating at Cascadia lacks the resolution for distinguishing between two ways of rupturing the entire length of the subduction zone: did the zone rupture in a single earthquake of $M_w$ 9 or did it break in a series of $M_w$ 8 earthquakes as much as a few decades apart [*Nelson et al.*, 1995]? Tsunami heights in Japan can answer this question because they are expected to differ about tenfold between a distant earthquake of tsunami magnitude ($M_t$) 8.0 and one of $M_t$ 9.0 [*Abe*, 1979, 1989]. Using Abe's tsunami magnitude formula, *Satake et al.* [1996] estimated that the 1700 Cascadia earthquake attained $M_w$ 9. This estimate influences hazard assessments for Cascadia's plate-boundary earthquakes and their tsunamis [*Frankel et al.*, 2000; *Priest et al.*, 2000; *Petersen et al.*, 2002].

[5] In this paper we show that $M_w$ 9 remains the likely size of the 1700 Cascadia earthquake. We make this estimate more rigorous in several ways. First, we present three sets of tsunami height estimates, namely, the estimates made by *Tsuji et al.* [1998] and two that we estimated from descriptions of damage and flooding in Japan using a very conservative approach and a less conservative approach. We use various assumptions and corrections in translating these descriptions into tsunami heights. Second, to represent sources of the 1700 tsunami, we use coseismic seafloor deformation computed with a three-dimensional (3-D) elastic dislocation model modified from that of *Wang et al.* [2003]. We make this computation for a unit amount of slip in six rupture models that differ in length, width, and downdip slip distribution. Finally, we numerically simulate tsunami propagation across the Pacific Ocean to estimate slip for each rupture model and to determine which model yields the best agreement with tsunami heights in Japan. Matching the three sets of tsunami height estimates from historical documents with the six rupture models, we obtain 18 combinations that together imply $M_w$ 8.7–9.2 as the size of the 1700 Cascadia earthquake. We discount at least half these combinations as inconsistent with paleoseismological evidence along the Cascadia coast. Among the remaining combinations, a rupture 1100 km long in an earthquake of $M_w$ 9.0 gives the best fit to our best estimates of tsunami heights in Japan.

## 2. Tsunami Heights in Japan

[6] The 1700 Cascadia tsunami probably crested 1–5 m above ambient tide among seven sites along nearly 1000 km of Japan's Pacific coast (Figure 2). These heights are interpretations of damage and flooding reported in old documents (Table 1). The height estimates include various combinations of assumptions and corrections (Tables 2 and 3a–3c). We present three sets of estimates for the 1700 tsunami: one set previously reported [*Tsuji et al.*, 1998] and two newly derived ("low" and "medium"). For each site we also summarize well-documented inundation by the tsunami from the 1960 Chile earthquake ($M_w$ 9.5); several of our medium estimates depend on the assumption that the 1700 tsunami crest descended inland as did the 1960 tsunami. As examples, we discuss heights of the 1700 and 1960 tsunamis at Miyako Bay, where old documents describe the 1700 tsunami as it affected the villages of Kuwagasaki and Tsugaruishi (Figures 3–5).

### 2.1. Descriptions of the 1700 Tsunami and Inference of Height

[7] Japanese descriptions of the 1700 tsunami, summarized in Table 1, show that it caused trouble onshore and offshore. It flooded farmed fields, ruined salt kilns, damaged fishermen's shacks, ascended a castle moat, entered a government warehouse, drove people to high ground, and probably ran 2 km up a river. It wrecked houses not only by flooding them but also by starting a fire. It contained multiple waves that range in reported time from midnight until the following noon. The tsunami initiated a nautical accident in which were lost two crew members and tons of rice.

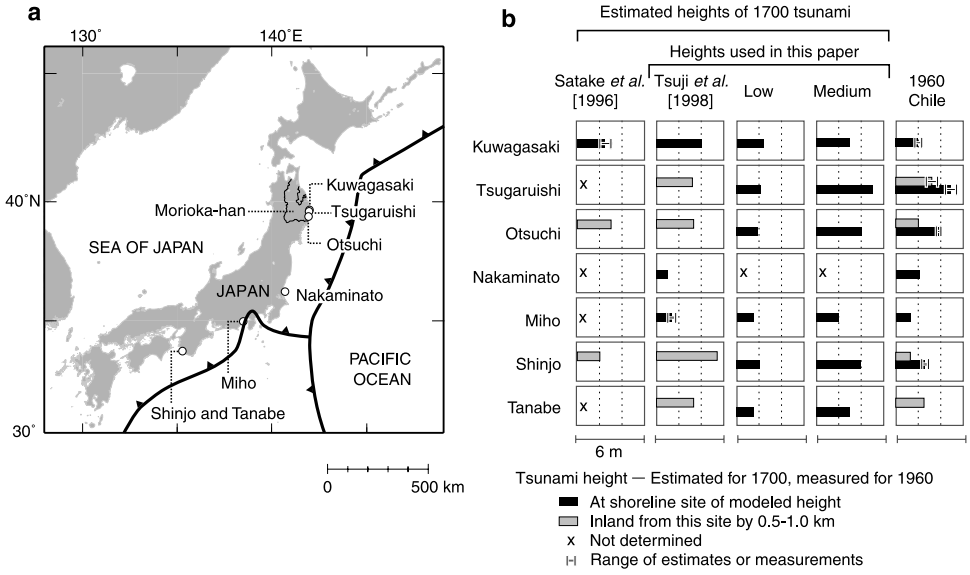


**Figure 2.** (a) Tectonic setting of Japan and locations where the 1700 tsunamis were documented. (b) Five sets of heights for the 1700 tsunami in Japan estimated from damage and flooding described in historical documents (Table 1). For the three sets used in this paper, criteria are defined in Table 2 and components are listed in Tables 3a–3c. Measured tsunami heights for the 1960 Chile earthquake of $M_w$ 9.5 show site-to-site variation mimicked only by the medium height set.

[8] To convert these reported effects into estimated heights, *Tsuji et al.* [1998] measured modern heights of places probably reached by the tsunami, assumed water depths responsible for damage to houses, corrected for tectonic land-level change since 1700, and corrected for tide stage at the time when the tsunami may have crested (Table 3a). In addition, they assumed no difference between tsunami height inland (at sites of damage or limits of flooding) and tsunami height at the nearest shore (the place for which we compute tsunami heights in section 4). The *Tsuji et al.* [1998] estimates vary with location in a pattern unlike that of the 1960 tsunami (Figure 2).

[9] Our low estimates, the smallest and most uniform, depend on assumptions that are conservative and uniform (Figure 2). For land where damage or flooding occurred in 1700, we assume a minimum height relative to high tides of that era and we assume a water depth barely sufficient to cause the damage or make the flooding noteworthy (Table 3b). Like the heights estimated by *Tsuji et al.* [1998], the low estimates include corrections for tide stage and exclude corrections for landward changes in onshore tsunami height. Because the low estimates refer directly to sea level in 1700, they circumvent adjustments for post-1700 changes in land level relative to sea level.

[10] The medium heights are our preferred estimates from criteria tailored to each site (Table 3c). A key assumption for three sites, Tsugaruishi, Otsuchi, and Shinjo, is that the maximum height of the 1700 Cascadia tsunami was greater at the shoreline than it was at sites of damage and flooding hundreds of meters inland. To estimate the inland decrease in tsunami height in 1700, we use the decrease measured for the Chile tsunami in 1960. This adjustment increases, by 1 m or more, the estimated height of the 1700 tsunami at the shoreline. The resultant variation among the medium heights improves agreement with computed heights, as shown in section 5.

### 2.2. Examples From Miyako Bay

[11] Accounts of the 1700 tsunami at Miyako Bay focus on its effects at Kuwagasaki and Tsugaruishi (Figure 3). Government records of Morioka-han, an administrative region in northern Japan (Figure 2a), state that in Kuwagasaki the 1700 waves came at midnight and directly destroyed 13 houses (Figure 4). Records of a merchant family mention the loss of houses in an unspecified area near the south end of Miyako Bay. The merchant account also describes flooding and consequent turmoil in Tsugaruishi village, 1 km inland from the bay, and refers to a river crossing as a limit of flooding. With the aid of a 1739 map, we locate this crossing about 2 km inland from Miyako Bay (the inundation limit in Figure 3).

[12] *Tsuji et al.* [1998] estimated tsunami heights of ~4 m at Kuwagasaki and 3.2 m at Tsugaruishi (Table 3a). In their estimate for Kuwagasaki, illustrated in Figure 5a, they assumed that the 13 destroyed houses had stood on land now 1.4–1.9 m above Tokyo Peil (TP), a datum close to modern mean sea level (MSL). For the midnight waves, they computed a tide level of 0.2 m below 1700 MSL, and from the destruction of houses they inferred a water depth of 1.0–1.5 m. Finally, by extrapolating tide-gauge data from the last half of the twentieth century, they estimated that the land had subsided 1.0 m in the three centuries since 1700. In their estimate for Tsugaruishi, *Tsuji et al.* [1998] used the present elevation of an area near the reported limit of the 1700 tsunami in that village, and they assumed the same tidal and tectonic corrections as for Kuwagasaki. They applied this inland height to inundation at the shore of Miyako Bay, 1 km seaward.

**Table 1.** Japanese Descriptions of the 1700 Tsunami and Its Effects[a]

| Place (Listed From North to South) | Documents | Account[b] |
|---|---|---|
| Kuwagasaki (39°39′N, 141°58′E) | Official daily records of feudal domain, compiled in domain's capital city 100 km inland from coast. | A tsunami struck Kuwagasaki around midnight of 27–28 January. Water destroyed 13 houses outright and set off fires that destroyed 20 more. People fled to high ground; none were injured. Emergency rice was issued to 159 people, and lumber was requested for reconstruction. *Account based on correspondence from district magistrates in Miyako, 1 km from Kuwagasaki. The 33 buildings destroyed probably represented over 10% of the village's housing stock.* |
| Tsugaruishi (39°35′N, 141°57′E) | Copy, probably a summary, of a merchant family's records, written in Tsugaruishi. | High saltwater washed away buildings, caused turmoil in Tsugaruishi village, and reached a river crossing. According to hearsay, the same high water set off fire that burned "about 21 houses" in Kuwagasaki. All this happened without an earthquake in the area. *Tsugaruishi village is 1 km from Miyako Bay, and the river crossing probably another 1 km farther inland. Because of an error in copying, the document dates the flooding 1 month before 27–28 January.* |
| Otsuchi (39°21′N, 141°55′E) | 1. Same book as Kuwagaski account. 2. Summary of records of district magistrate in Otsuchi. | A high tide came at midnight of 27–28 January (document 1). The water damaged rice paddies and vegetable fields seaward of the town's main street, as well as two fishermen's buildings and two salt kilns (1). No people or horses were injured (2). *The account in (1) is based on the correspondence from the district magistrate in Otsuchi. The summary in (2) gives the same hour, day, and year; it omits the month, probably from an error in copying.* |
| Nakaminato (36°21′N, 140°36′E) | Shipwreck documents collected in the nineteenth century by a family in the shipping business in Nakaminato. | Around 0800 LT on 28 January, "high waves" prevented a rice boat from entering the port of Nakaminato. The crew cast anchor offshore. That evening, a storm set the boat adrift. Eventually lost were the boat, its cargo (28 t of rice), and two of the crew. *The high waves may have been ocean swells opposed by strong ebb currents from drawdown between tsunami wave crests. In Nakaminato's harbor, the 1960 tsunami created an ebb current estimated to have exceeded 7 knots (3.5 m/s).* |
| Miho (35°00′N, 138°31′E) | Anthology, selected and copied in the 1800s, of village-headmen's records of Miho. | Seven waves occurred in the morning of 28 January, between dawn and about 1000 LT. Each wave rose gradually, and each went out like a river. The water entered a pine grove. It rose inside a bay but not on a nearby beach. Children and the elderly were advised to go to high ground. No earthquake was felt in Miho or nearby. The waves puzzled the villagers. |
| Tanabe (33°44′N, 135°24′E) and Shinjo (33°43′N, 135°24′E) | Official record of the castle town of Tanabe, and parallel private record of the town's hereditary mayor. | Unusual seas began by dawn on 28 January. The water entered a government storehouse "and so on" in Shinjo village. In Shinjo and several other villages, it damaged rice paddies and wheat crops. In Tanabe itself, the water ascended a castle moat to within 150 m of the mayor's home. *Shinjo, 3 km from Tanabe castle, belonged to a district administered by Tanabe's mayor. The storehouse in Shinjo probably contained bails of rice that had been collected as tax. The name used for the storehouse implies ownership by a main branch of Japan's ruling Tokugawa family. A tsunami in 1707 destroyed two government storehouses in Shinjo, one of which may have been the one flooded in 1700.* |

[a]Main source is *Tsuji et al.* [1998].
[b]Authors' comments in italics.

**Table 2.** Criteria for Various Estimates of Tsunami Height

| | *Satake et al.* [1996] | *Tsuji et al.* [1998] | Low | Medium |
|---|---|---|---|---|
| Infer height from damage and extent | x | x | x | x |
| Correct for astronomical tide | | x | x | x |
| Measure present height of flooded site | | x | | x |
| Correct for land-level change since tsunami | | x | | x |
| Correct for onshore slope of tsunami | | | | x |
| Use 1960 Chile tsunami as proxy for 1700 | | | | x |

**Table 3a.** Basis for Height Estimates by *Tsuji et al.* [1998][a]

| Place | A: Present Height of Inundated Site (m Above TP) | B: Assumed Depth of Tsunami at Inundated Site, m | C: Inferred Tide During Tsunami (m Above 1700 MSL) | D: Net Emergence Since 1700, m | E: Height Above Tide During Tsunami (A + B − C − D), m |
|---|---|---|---|---|---|
| Kuwagasaki | 1.4–1.9 | 1.0–1.5 | −0.2 | −1.0 | ∼4 |
| Tsugaruishi | 2.0 | 0 | −0.2 | −1.0 | 3.2 |
| Otsuchi | 1.6 | 0 | −0.2 | −1.5 | 3.3 |
| Nakaminato | no onshore inundation | no onshore inundation | correction not used | correction not used | ∼1 |
| Miho | 1.6 | 0 | −0.2 | 0.1–0.8 | 1.0–1.7 |
| Shinjo | 4.1 | 0 | −0.3 | −1.0 | 5.4 |
| Tanabe | 2.0 | 0 | −0.3 | −1.0 | 3.3 |

[a]TP is Tokyo Peil, a datum close to modern mean sea level. Heights in column E assumed to apply to nearest shoreline, whether determined for places within about 0.1 km of the shore (Kuwagasaki and Miho) or for sites farther inland (Tsugaruishi 1.0 km, Otsuchi 0.5 km, Shinjo 0.7 km, Tanabe 0.5 km). Height for Nakaminato based on reported disruption to shipping and on analogous disruption during twentieth century tsunamis.

[13] Our low height estimates are smaller than those of *Tsuji et al.* [1998] and differ little between Kuwagasaki (2.4 m) and Tsugaruishi (2.2 m) (Table 3b). For both estimates we assume that the destroyed houses stood on land at least 0.5 m above the highest tides of 1700, a datum we estimate as 0.7 m above 1700 MSL by analogy with modern tide data (Figure 5b). For destruction of houses we assume a flow depth of 1.0 m. We adjust for tide level at the time of tsunami arrival for Kuwagasaki but not for Tsugaruishi, where the merchant's document, a summary, gives no times.

[14] Only our medium height estimates show a pattern similar to that of the 1960 Chile tsunami, which was lower at Kuwagasaki than on the Miyako Bay coast near Tsugaruishi (Figure 3). The 3-m medium height at Kuwagasaki (Figure 5c) is a compromise between the ∼4 m of *Tsuji et al.* [1998] (in which the extrapolated tectonic correction may be excessive) and our low estimate of 2.4 m (which contains conservative estimates of land height and water depth). At the head of Miyako Bay near Tsugaruishi, a height of 5 m was reached in many places by the 1960 tsunami (Figure 3) [*The Committee for Field Investigation of the Chilean Tsunami of 1960*, 1961, pp. 178–179]. We use 5 m as the medium height for the 1700 tsunami because, as shown in the next two paragraphs, the 1960 and 1700 tsunamis probably had similar limits upriver from Tsugaruishi and because Miyako Bay amplifies long-period tsunamis.

[15] The 1960 tsunami inundation limit along the Tsugaruishi River is within several hundred meters of the limit we infer for the 1700 tsunami. From the south shore of Miyako Bay, the 1960 tsunami ran 1 km inland to Tsugaruishi village, where its maximum level was about 3–4 m above TP, as inferred from inundation limits shown to us by an eyewitness in 1999. From the village it continued another 1 km farther up the Tsugaruishi River [*Kon'no*, 1961, p. 22; *The Committee for Field Investigation of the Chilean Tsunami of 1960*, 1961, p. 239, 259]. The inundation limit of the 1700 tsunami, as described above, was probably also about 2 km from the bay.

[16] Miyako Bay, with a seiche period of 45 min, amplified long-period waves of the 1960 Chile tsunami [*Kato et al.*, 1961]. Shaped like a finger, the bay extends about 10 km from its mouth near Kuwagasaki to its head near Tsugaruishi (Figure 3). The 1960 Chile tsunami, with an average period of about 1 hour, reached maximum heights of about 2 m near Kuwagasaki but approached 6 m at the shore near Tsugaruishi [*The Committee for Field Investigation of the Chilean Tsunami of 1960*, 1961, pp. 178–179]. We assume that without such amplification the 1700 tsunami could not have run 2 km inland from the south shore of the bay.

## 3. Fault Models

[17] We compute seafloor deformation for six rupture models that differ in dimensions and location. The along-strike length and downdip width for each rupture model are consistent with current understanding of plate-boundary geometry and modern interseismic deformation. Three of the model ruptures extend the full 1100 km length of the subduction zone. We make one of these ruptures wide to examine the effect of downdip slip distribution on the Japanese tsunami heights. We also consider three shorter ruptures to examine how much slip they require to repro-

**Table 3b.** Basis for the Low Height Estimate[a]

| Place | A: Highest Astronomical Tide (m above MSL) | B: Assumed Height of Site Above Tide in A, m | C: Assumed Depth of Tsunami at Inundated Site, m | D: Inferred Tide During Tsunami (m above 1700 MSL) | E: Height Above Tide During Tsunami (A + B + C − D), m |
|---|---|---|---|---|---|
| Kuwagasaki | 0.7 | 0.5 | 1.0 | −0.2 | 2.4 |
| Tsugaruishi | 0.7 | 0.5 | 1.0 | 0 | 2.2 |
| Otsuchi | 0.7 | 0.5 | 0.5 | −0.2 | 1.9 |
| Miho | 0.8 | 0.5 | 0.3 | 0 | 1.6 |
| Shinjo | 1.0 | 0.5 | 0.3 | −0.3 | 2.1 |
| Tanabe | 1.0 | 0 | 0.3 | −0.3 | 1.6 |

[a]Because of small tidal ranges, extreme tide in column A is only a few tenths of a meter above mean high water. Height in column B allows buildings and trees to escape routine attack by wind waves at high tide. Depths in column C: minimum of 1.0 m to destroy buildings, 0.5 m to damage buildings, 0.3 m to enter pines and storehouse and to ascend moat to its inland end. Tides in column D computed for reported midnighttime of flooding (Kuwagasaki, Otsuchi), onset of observed flooding (dawn at Shinjo, Tanabe), or approximate midpoint of tide range during many-hour interval of flooding (Tsugaruishi, 2 days; Miho, 0600–1000 local time). Total in column E excludes any correction for water-surface slope.

**Table 3c.** Basis for the Medium Height Estimate[a]

| Place | Low (Table 3b) | Medium | Main Reasons Why Medium Height Exceeds Low Height |
|---|---|---|---|
| Kuwagasaki | 2.4 | 3 | Damage in 1700: some of the 13 houses destroyed directly by the tsunami may have been founded more than 0.5 m above extreme high tide or may have been flooded by water deeper than 1.0 m. Comparison with 1677: a large local tsunami in 1677 destroyed only five houses in Kuwagaski. |
| Tsugaruishi at south end of Miyako Bay | 2.2 | 5 | Analogy with 1960 tsunami: the 1700 and 1960 tsunamis both ran about 2 km up the Tsugaruishi River. The 1960 tsunami averaged 5 m high at south end of Miyako Bay. |
| Otsuchi at Otsuchi Bay | 1.9 | 4 | Tectonic subsidence since 1700: areas probably reached by the 1700 tsunami, now about 2 m above mean sea level, may have stood 1.5 m higher in 1700 (Table 3a). Analogy with 1960 tsunami: the 1700 and 1960 tsunamis both terminated in the same area about 0.5 km inland from Otsuchi Bay. At the bay shore, the 1960 tsunami had a height range 3.6–4.0 m. |
| Miho | 1.6 | 2 | No additional height inferred. |
| Shinjo at Mori Harbor | 2.1 | 4 | Analogy with 1960 tsunami: at its traditional site, the Shinjo storehouse was about 0.7 km inland from the present shore of Mori Harbor. Across this distance, the 1960 tsunami height decreased about 1.0–1.5 m. |
| Tanabe near mouth of Aizu River | 1.6 | 3 | Flooding in 1700: water in moat may have risen a meter or two above the minimal level inferred in Table 3b. Such a rise is consistent with the reported flooding of fields and crops near Tanabe. |

[a]Medium height is rounded to nearest whole meter.

duce the Japanese tsunami and to see whether such slip is tectonically and paleoseismologically reasonable.

[18] In all cases we assume that the slip is continuous and smooth, without asperities. Because it is also instantaneous, the resulting seafloor deformation fully contributes to tsunami generation. We use an elastic dislocation model, in which the slip is prescribed [*Flück et al.*, 1997; *Wang et al.*, 2003]. We do not try representing the fault ruptures in a crack model, where the slip distribution is computed with an assumption of constant stress drop [*Geist and Dmowska*, 1999]. The amount of fault slip for each dislocation model is determined by minimizing disagreement between the estimated tsunami heights from section 2 and the computed heights from section 4.

### 3.1. Three-Dimensional Elastic Dislocation Model

[19] Our computation of coseismic seafloor deformation uses the 3-D interseismic dislocation model of *Wang et al.* [2003]. Geodetic measurements of modern interseismic deformation of the Cascadia forearc have been used to constrain 3-D elastic dislocation models [*Flück et al.*, 1997; *Wang et al.*, 2003] and a 3-D viscoelastic finite element model [*Wang et al.*, 2001]. In the dislocation models, which numerically integrate point source solutions over the curved subduction thrust fault, the fault is divided into a locked zone with a uniform back slip rate and a transition zone over which the back slip rate decreases downdip. To set the downdip limit of the locked zone, the models depend on thermal data [*Hyndman and Wang*, 1995] and, secondarily, on geodetic observations.

[20] To calculate coseismic seafloor deformation, we divide the area of coseismic slip into a ''full-slip zone'' and a ''partial-slip zone'' (Figure 6). In most of our models, the full-slip zone spans the same downdip width as the interseismic locked zone. We assume that the full-slip zone ruptured completely during the 1700 earthquake. In the

**Table 3d.** Height Measurements of the 1960 Chile Tsunami[a]

| Place | A: Measured Height at Inland Site of 1700 Inundation (m above TP) | B: Measured Height at Nearest Shoreline (m above TP) | C: Landward Decrease in Tsunami Height (B − A), m | D: Measured Tide During Tsunami, (m above 1960 MSL) | E: Height Inland, Relative to Tide During Tsunami (A − D), m | F: Height at Shoreline, Relative to Tide During Tsunami (B − D), m |
|---|---|---|---|---|---|---|
| Kuwagasaki | 1.8–2.4 | 1.8–2.4 | 0 | 0.1 | 1.7–2.3 | 1.7–2.3 |
| Tsugaruishi | ~3.3 at Inari-shita | 4.5–5.5 | 1.0–2.0 | 0.1 | ~3.2 | 4.4–5.4 |
| Otsuchi | ~2 near inland limit of 1700 tsunami | 3.6–4.0 | 1.5–2.0 | 0 | ~2 | 3.6–4.0 |
| Nakaminato | 2.1 | no coastal data | no data | 0 | 2.1 | no data |
| Miho | 1.6 | 1.6 | no data | 0.3 | 1.3 | no data |
| Shinjo | 2.1 near traditional site of storehouse | 3.1–3.7 | 1.0–1.5 | 0.8 | 1.3 | 2.3–2.9 |
| Tanabe | 3.3 along river ~0.3 km from site | no coastal data | no data | 0.8 | 2.5 | no data |

[a]TP is Tokyo Peil, a datum close to modern mean sea level. Difference in column C is rounded to nearest 0.5 m.

**Table 3e.** Comparison Among the Height Estimates

| Place | A: *Satake et al.* [1996] | B: *Tsuji et al.* [1998] (Table 3a) | C: Low (Table 3b) | D: Medium (Table 3c)[a] | E: 1960 Chile (Table 3d) |
|---|---|---|---|---|---|
| Kuwagasaki | 2–3 | ~4 | 2.4 | 3 | 1.7–2.3 |
| Tsugaruishi at Inari-shita | ... | 3.2 | ... | ... | ~3.2 |
| Tsugaruishi at Miyako Bay | ... | ... | 2.2 | 5 | 4.4–5.4 |
| Otsuchi near inland limit of 1700 tsunami | 3 | 3.3 | ... | ... | ~2 |
| Otsuchi at Otsuchi Bay | ... | ... | 1.9 | 4 | 3.6–4.0 |
| Nakaminato | ... | ~1 | ... | ... | 2.1 |
| Miho | ... | 1.0–1.7 | 1.6 | 2 | 1.3 |
| Shinjo near traditional site of storehouse | 2 | 5.4 | ... | ... | 1.3 |
| Shinjo at Mori Harbor | ... | ... | 2.1 | 4 | 2.3–2.9 |
| Tanabe at Horidobashi | ... | 3.3 | ... | ... | ... |
| Tanabe near mouth of Aizu River | ... | ... | 1.6 | 3 | 2.5 |

[a]Column D is rounded to nearest whole meter.

partial-slip zone, downdip from the full-slip zone, coseismic slip diminishes to zero at a distance halfway down the interseismic transition zone [*Wang et al.*, 2003]. The coseismic partial-slip zone should be narrower than the interseismic transition zone because the latter partly serves to simulate postseismic viscoelastic stress relaxation.

[21] The downdip limit of coseismic rupture has modest effects on coseismic seafloor deformation and the resulting tsunami. This insensitivity is shown in section 5 by similarities between tsunamis computed with the Long-Narrow and Long-Wide models, which differ only in the downdip extent of full slip. However, these two models predict distinctly different patterns of coseismic vertical deformation along the coast, where the patterns can be compared with paleoseismological evidence (section 6).

[22] The direction of coseismic slip is assumed opposite to the northeastward motion of the Juan de Fuca plate relative to the Cascadia forearc (Figure 1). *Wang et al.* [2003] estimated Juan de Fuca-Cascadia forearc convergence by using the Cascadia forearc-North America pole defined by *Wells and Simpson* [2001] and a Juan de Fuca-North America pole consistent with the Pacific-North America pole of *DeMets and Dixon* [1999]. The Euler pole for Pacific-North America convergence [*DeMets and Dixon*, 1999] predicts oblique Juan de Fuca-North America convergence with a significant along-strike variation in convergence rate. Using geological data, *Wells et al.* [1998] and *Wells and Simpson* [2001] found that the Cascadia forearc roughly south of the Canada-United States border rotated clockwise and translated northwestward relative to North America in the late Cenozoic. Such forearc motion is consistent with the forearc stress pattern [*Wang*, 1996]. GPS observations confirm that this forearc motion still continues [*Savage et al.*, 2000; *McCaffrey et al.*, 2000; *Miller et al.*, 2001].

[23] The amount of slip on the fault varies less along its strike than down its dip. Slip amount changes slightly along strike because its distribution is defined by the Euler poles. Averaging along strike gives the average slip of the full-slip zone. Slip decreases linearly downdip across the partial-slip zone. Averaging over the entire rupture area, across the full-slip zone and the partial-slip zone, gives the average slip of the earthquake, which is less than the average in the full-slip zone alone.

[24] These different average amounts of slip have different uses (section 5.3). To calculate seismic moment, we use the slip averaged over both the full-slip zone and the partial-slip zone. To compare coseismic slip with interseismic plate convergence, however, we use only the slip on the full-slip zone. In this comparison, we assume that slip in 1700 did not necessarily recover all the slip deficit that had accumulated beforehand.

### 3.2. Rupture Models

[25] Three of six rupture models span the entire 1100 km length of the Cascadia subduction fault: Long-Narrow, Long-Splayed, and Long-Wide (Figures 7 and 8). In the other three models, Short-North, Short-Central, and Short-South, rupture is limited to hypothetical segments of the Cascadia fault (Figure 8).

[26] The Long-Narrow model comprises full-slip and partial-slip zones that have average downdip widths of 48 and 51 km, respectively (Figure 7a). With their slip

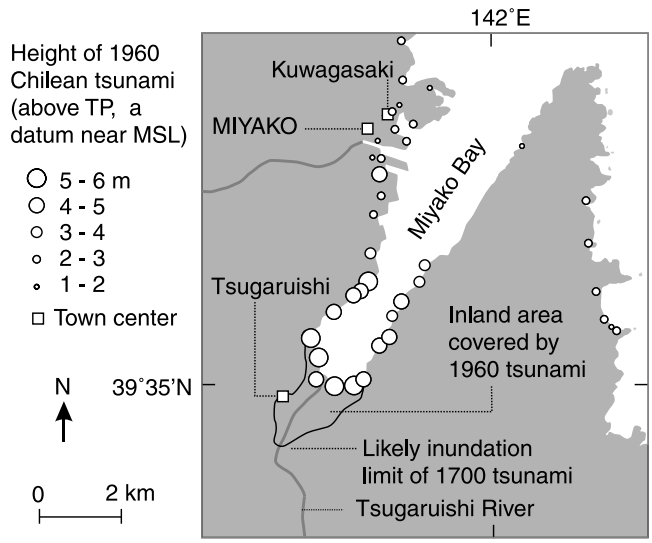


**Figure 3.** Miyako Bay, where the 1700 tsunami is known to have entered villages of Kuwagasaki and Tsugaruishi. Symbols show measured heights of the 1960 Chile tsunami as reported by the *Committee for Field Investigation of the Chilean Tsunami of 1960* [1961, pp. 178–179]. From the south end of Miyako Bay, the 1700 tsunami went inland about as far as did the 1960 tsunami [*Kon'no*, 1961, p. 22; *Committee for Field Investigation of the Chilean Tsunami of 1960*, 1961, pp. 239, 259].

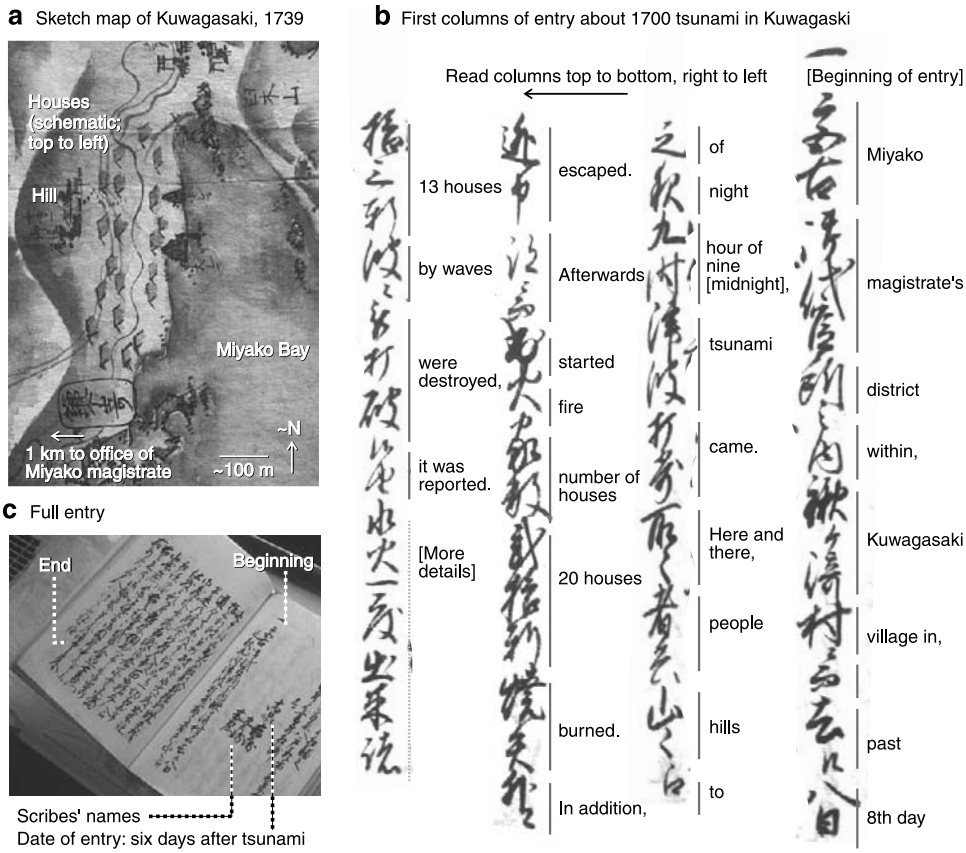


**Figure 4.** Description of effects of the 1700 tsunami on the village of Kugawasaki. (a) Sketch map of Kugawasaki. (b) First columns of entry about the 1700 tsunami, as recorded in "*Morioka-han Zassho*," official records from northern Japan. (c) Pages of "*Morioka-han Zassho*," of the volume for the twelfth year of Genroku era, which includes January 1700. Government officials in Morioka based the description on correspondence from magistrates stationed in Miyako, 1 km from Kuwagasaki. The map and the book are courtesy of Morioka City Central Community Center, where they are archived.

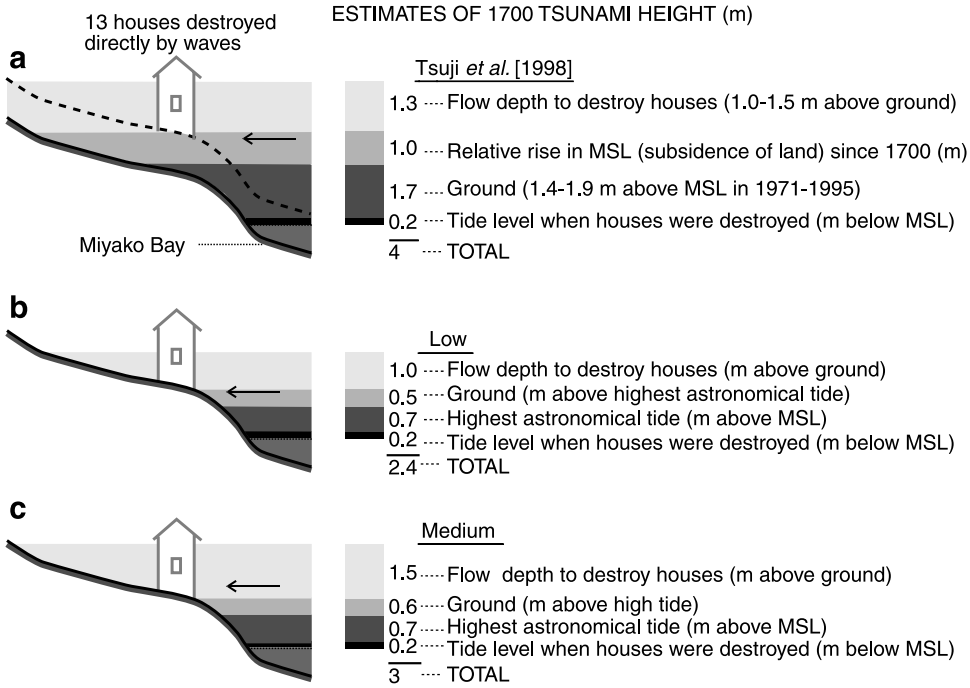


**Figure 5.** Cartoons showing ingredients of three estimates of 1700 tsunami height at Kuwagasaki. (a) *Tsuji et al.* [1998], (b) low estimate, and (c) medium estimate.

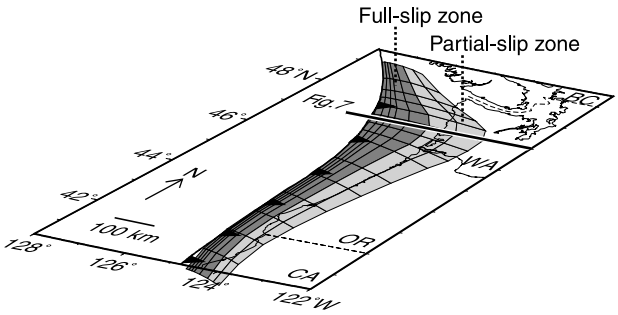


**Figure 6.** Three-dimensional view of the fault geometry used in the Long-Narrow model (modified from *Wang et al.* [2001]).

averaged along strike, these two zones are equivalent to a uniform full-slip zone 74 km wide (Table 4), which is used to calculate the seismic moment. Slip in the Long-Narrow model causes uplift of the ocean bottom and subsidence of the coastal region above the partial-slip zone. The seaward edge of the uplift forms a narrow ridge near the upper end of the full-slip zone. This ridge results from sharp truncation of uniform slip at the shallow end; the ridge diminishes if the slip decreases near the rupture zone's updip end, and it disappears if uniform rupture continues to the ocean bottom. Realistic or not, such a ridge has little effect on computed tsunami heights at Cascadia [*Priest et al.*, 2000] and even less effect on computed tsunami heights in Japan.

[27] To examine the effects of the geometry and width of long ruptures, we modify the Long-Narrow model into Long-Splayed and Long-Wide models. In the Long-Splayed model, the most seaward 10 km of the rupture zone, instead of following the plate interface as in the Long-Narrow model, extends upward to the seafloor as a linear splay fault (Figure 7b). The same uniform slip is applied to this splay as to the rest of the full-slip zone, farther downdip. The splay fault increases coseismic uplift near the deformation front. The equivalent uniform width is 75 km, similar to that of the Long-Narrow model. The Long-Wide model is derived by imposing uniform slip on both the full-slip and partial-slip zones of the Long-Narrow model (Figure 7c). The average rupture width for the Long-Wide model is 100 km. This model leads to a wider area of seafloor uplift. The center of the coseismic subsidence is shifted landward, and the maximum coastal subsidence is greater.

[28] How much seismic slip on shorter Cascadia ruptures would suffice to produce the 1700 tsunami in Japan? To explore this question, we consider three hypothetical ruptures 360–670 km long (Figure 8). For these ruptures we use segment boundaries inferred by *Wells et al.* [2003] from forearc basins, and we use full-slip and partial-slip zones from the appropriate along-strike part of our Long-Narrow model. The rupture in our Short-North model extends 670 km northward from a proposed boundary at 44.3°N latitude off central Oregon. This model rupture spans most of the subduction zone off northern Oregon, Washington, and British Columbia (Figure 8d). A shorter version of the Short-North rupture, called Short-Central, covers 360 km of the subduction zone between central Oregon and a potential segment boundary at the latitude of the Olympic Peninsula (Figure 8e) [*Wells et al.*, 2003]. The last model, Short-South, extends 440 km southward from central Oregon to northern California (Figure 8f). The equivalent uniform rupture widths for the Short-North, Short-Central, and Short-South models are 87, 91, and 56 km, respectively. The rupture is wider in the Short-North and Short-Central models than in the Short-South model because the subduction fault dips most gently beneath Washington (Figures 1 and 6). The best dated of the paleoseismological evidence for the 1700 earthquake comes from the area covered by the Short-North and Short-Central models (Figures 1 and 8).

## 4. Tsunami Computations

[29] Our computations of the 1700 Cascadia tsunami begin with sea surface displacement that matches the underlying seafloor deformation calculated from the 3-D

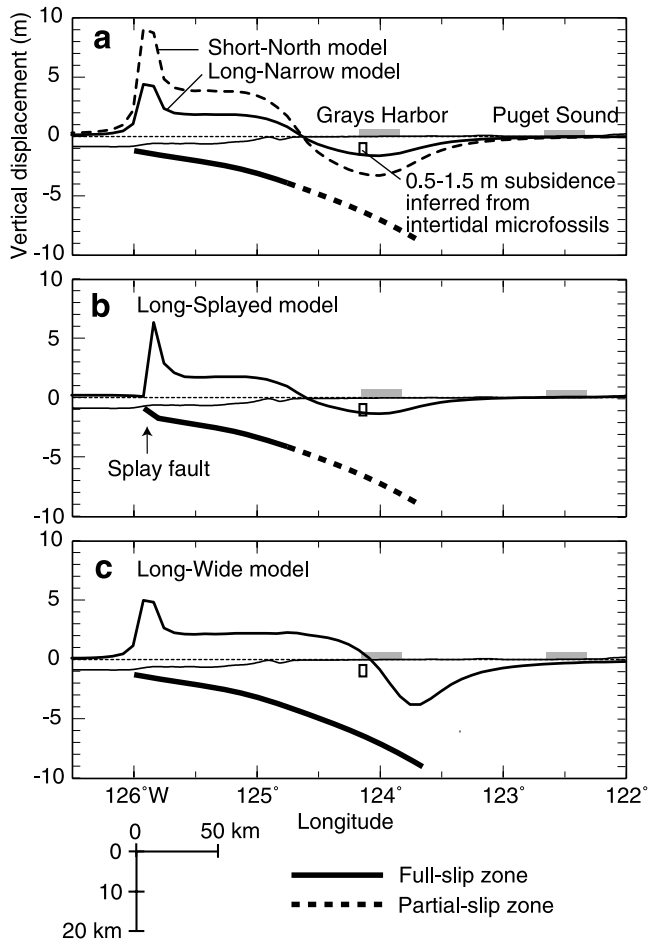


**Figure 7.** Cross section through southern Washington (at 47°N: Figure 6) illustrating three different downdip slip distributions and the vertical coseismic deformation computed from them. (a) In the Narrow model (used for the Long-Narrow and all short rupture models), the slip decreases linearly downdip in the partial-slip zone. (b) A linear splay fault connects the seafloor with the main thrust in the Long-Splayed fault model. (c) Full slip is assumed over the entire fault width in the Long-Wide rupture model.

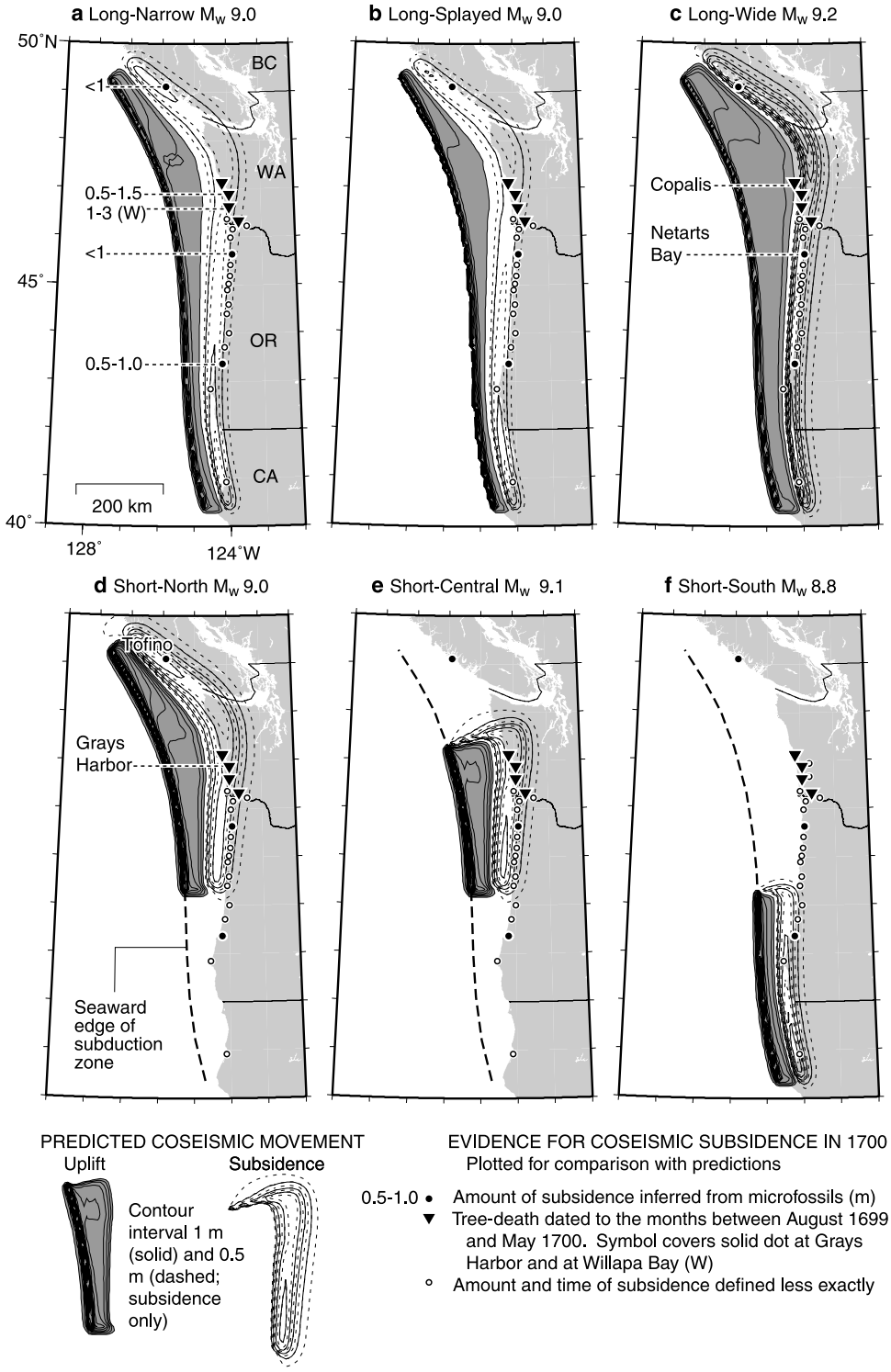


**Figure 8.** Computed vertical deformation patterns for the six rupture models (Table 4). (a) Long Narrow, (b) Long-Splayed, (c) Long-Wide, (d) Short-North, (e) Short-Central, and (f) Short-South models. The moment magnitudes computed for the 1700 medium tsunami height estimates are indicated in each rupture model. The solid curves indicate uplift and subsidence with a contour interval of 1 m. The dashed curves are subsidence with a contour interval of 0.5 m. Some of the computed patterns agree with paleoseismological evidence (Figures 8a and 8b), while others do not (Figures 8c–8f). Subsidence estimates from *Hemphill-Haley* [1995], *Nelson et al.* [1996, 1998], *Shennan et al.* [1996, 1998], *Guilbault et al.* [1996], and *Hughes et al.* [2002]; tree-death dating by *Yamaguchi et al.* [1997] and *Jacoby et al.* [1997]. Other sites of inferred subsidence from compilation by *Peterson et al.* [1997] and from *Kelsey et al.* [1998].

**Table 4.** Fault Parameters[a]

| | Long-Narrow | Long-Splayed | Long-Wide | Short-North | Short-Central | Short-South |
|---|---|---|---|---|---|---|
| | | | *Fault Size* | | | |
| Length, km | 1100 | 1100 | 1100 | 670 | 360 | 440 |
| Equivalent width, km | 74 | 75 | 100 | 87 | 91 | 56 |
| Full-slip zone width, km | 48 | 49 | 100 | 56 | 60 | 37 |
| | | | *Tsuji et al.* [1998] *Heights* | | | |
| Average slip, m | 13 | 13 | 20 | 27 | 31 | 21 |
| Full-slip zone slip, m | 18 | 17 | 20 | 37 | 42 | 28 |
| Seismic moment, $10^{22}$ N m | 4.3 | 4.2 | 8.7 | 6.3 | 4.1 | 2.0 |
| Moment magnitude, $M_w$ | 9.0 | 9.0 | 9.2 | 9.1 | 9.0 | 8.8 |
| | | | *Low Heights* | | | |
| Average slip, m | 8 | 8 | 12 | 17 | 19 | 13 |
| Full-slip zone slip, m | 11 | 11 | 12 | 23 | 26 | 17 |
| Seismic moment, $10^{22}$ N m | 2.6 | 2.6 | 5.3 | 3.9 | 2.5 | 1.2 |
| Moment magnitude, $M_w$ | 8.9 | 8.9 | 9.1 | 9.0 | 8.9 | 8.7 |
| | | | *Medium Heights* | | | |
| Average slip, m | 14 | 13 | 21 | 29 | 33 | 22 |
| Full-slip zone slip, m | 19 | 18 | 21 | 39 | 44 | 29 |
| Seismic moment, $10^{22}$ N m | 4.6 | 4.4 | 9.2 | 6.7 | 4.3 | 2.1 |
| Moment magnitude, $M_w$ | 9.0 | 9.0 | 9.2 | 9.1 | 9.0 | 8.8 |

[a]The definition of equivalent width is in accordance with the average slip of the earthquake.

dislocation model. To compute tsunami propagation across the Pacific Ocean and waveforms at shorelines in Japan, we use a finite difference method. As in other tsunami computations [e.g., *Johnson et al.*, 1996; *Satake*, 2002], the approach includes a linear long-wave approximation, adjustment for the Coriolis force, and gridded modern bathymetry. The results provide computed heights for comparison with heights estimated from descriptions of the damage and flooding in 1700 (section 2).

### 4.1. Linear Long-Wave Approximation

[30] In the long-wave approximation, tsunami wavelength far exceeds water depth. The approximation holds for most of the trans-Pacific path of the 1700 Cascadia tsunami because the ocean-bottom deformation that generated the tsunami had a wavelength of about 100 km (Figure 7), more than 20 times the average ocean depths along the tsunami's route to Japan. The linearity assumption means that tsunami amplitude is small compared with water depth and that bottom friction is therefore negligible. Because the 1700 tsunami had an amplitude no greater than a few meters, the linearity assumption is valid for the tsunami's crossing of the deep ocean, which makes up most of the propagation path (Figure 9). Linearity breaks down, however, in near-shore waters where the depth is comparable to the tsunami amplitude, including bays near Tsugaruishi and Shinjo. Linearity also breaks down where the tsunami inundates land.

[31] We make these computations linear for two reasons. First, nonlinear computations would require, and their results would depend upon, details of bathymetry, topography, land use, damage, and flooding. Few such details are available for the 1700 tsunami. Second, linear tsunami computations facilitate estimates of seismic slip. Under the linearity assumption, computed tsunami heights in Japan are proportional to initial water-surface displacement, which is assumed to be identical to coseismic seafloor displacement. The seafloor displacement, in turn, is proportional to seismic slip because our elastic dislocation modeling is linear. The assumption allows us to scale the results for each rupture model to fit the three sets of tsunami heights estimated from documentary descriptions.

### 4.2. Tsunami Computation in the Pacific Ocean

[32] To compute propagation of tsunami across the Pacific Ocean, we use modern bathymetry with a grid size of 5′ (about 9 km along a meridian), except for finer grids near Japan (section 4.3). The time step for computation is 5 s, small enough to satisfy the stability condition of the finite difference computation.

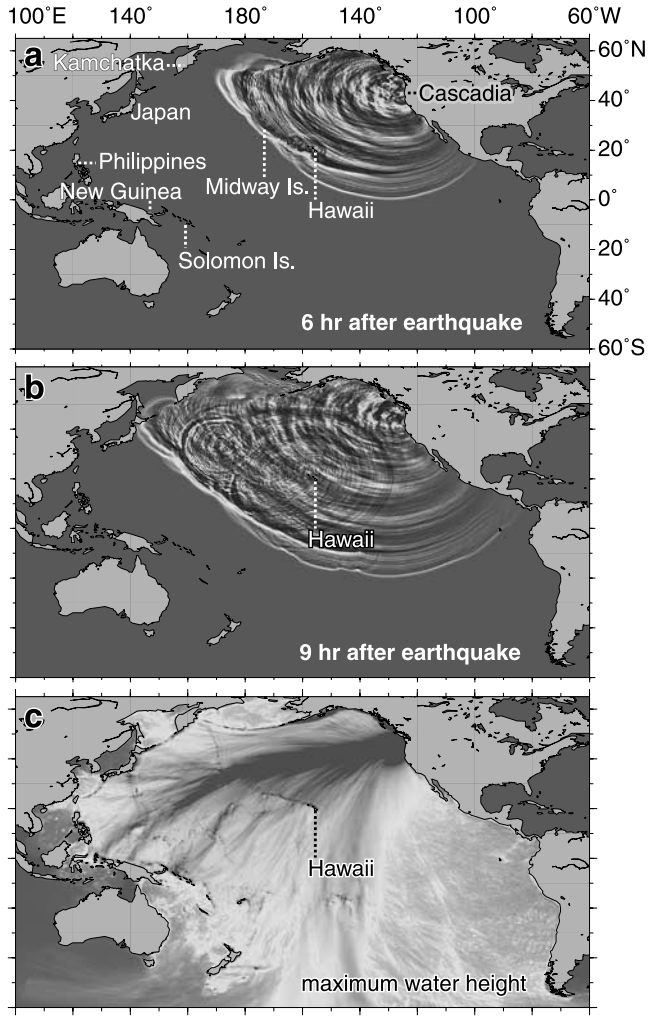


**Figure 9.** Tsunami computed for a $M_w$ 9.0 Cascadia earthquake with the Long-Narrow model. (a) At 6 hours, and (b) at 9 hours after the earthquake. (c) Maximum tsunami heights during the first 24 hours after the earthquake. Slip is 19 m in the full-slip zone and 14 m when averaged over full-slip and partial-slip zones. These snapshots are from color animation in the auxiliary material.

[33] The computed tsunami amplitudes vary with the azimuth of the path across the Pacific Ocean (Figure 9; see also auxiliary material[1]). Tsunami amplitudes are largest in the direction perpendicular to the fault strike [*Ben-Menahem and Rosenman*, 1972]. Especially for the long-rupture models, most tsunami energy from the Cascadia subduction zone is directed toward the northwestern Pacific Ocean (Figure 9c). Computed tsunami amplitudes are large in an arc between Hawaii and Kamchatka and are largest along a line toward the Midway Islands. Large amplitudes continue toward the Pacific coasts of Japan, Philippines, New Guinea, and Solomon Islands. Among all these places, only Japan has a wealth of documents from 1700.

### 4.3. Computed Waveforms in Japan

[34] To compute tsunami heights with an accuracy similar to that of the heights inferred from historical descriptions, we use a minimum grid size of 12″ (about 0.4 km) near Japan's Pacific coast. This minimum size is smaller than the 1′ (about 1.8 km) grids that have successfully simulated the waveforms, for the first hour or less, of twentieth century tsunamis that crossed the Pacific Ocean [e.g., *Johnson et al.*, 1996]. Maximum tsunami height, commonly several hours after the first arrival, can result from reflection at a coast or resonance within a bay, in response to local coastal shape and bathymetry. The 12″ grid has the advantage of showing these local effects. Because little of the reported damage and flooding in 1700 can be located more exactly than 0.4 km, 12″ may be the finest grid size for a meaningful computation. The computed tsunami heights represent the mean within each cell of the 12″ grid. For comparison with the heights estimated from damage and flooding (Namely, the Tsuji et al., low, and medium heights in section 2) we assign each estimated height to a shoreline site and compare it with the mean computed height for the cell that contains this site.

[35] In Miyako Bay (Figure 3), the tsunami waveforms vary less with source models than with nearshore amplification. At Kuwagasaki and also at Tsugaruishi, the computed tsunami waveforms are similar among rupture models (Figure 10). However, at Kuwagasaki, near the entrance of Miyako Bay, the waveforms have low amplitudes and a typical period of about 20 min, while near Tsugaruishi, at the inland end the bay, the computed waveforms have larger amplitudes, particularly at periods close to an hour. The waveforms thereby show resonance much like that observed for the 1960 Chile tsunami at Miyako Bay (section 2.2).

[36] The maximum computed heights may lag the first arrivals by as much as several hours (Figure 10). To compare with tsunami heights estimated from reported damage and flooding, we use maximum computed heights from broad ranges of times after the tsunami origin: 9–16 hours for Kuwagasaki southward to Miho and 11–18 hours for farther south at Shinjo and Tanabe.

## 5. Comparison of Tsunami Heights and Fault Parameters

[37] For each of the six rupture models (section 3), we estimate average fault slip that produces best agreement between computed heights (section 4) and the three sets of estimated tsunami heights (section 2) for a total of 18 combinations. Two statistical measures of similarity between estimated and computed tsunami heights show best agreement between the medium set and the Long-Narrow model (Figure 11). The best fit values for fault slip afford estimates of seismic moment and moment magnitude.

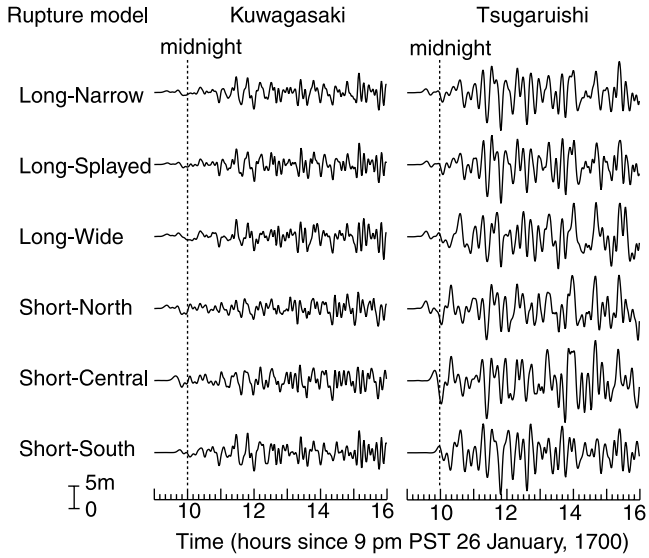


**Figure 10.** Computed tsunami waveforms at Kuwagasaki and Tsugaruishi (see Figure 3 for locations) for the six rupture models (Figure 8). Shown are waveforms 9–16 hours after the 1700 earthquake.

### 5.1. Statistical Measures of Agreement

[38] Two parameters, the error factor κ and the correlation coefficient $r$, measure the agreement between the heights estimated from descriptions and the heights computed from rupture models. Small values of κ (minimum of 1.0) and large values of $r$ (maximum of 1.0) denote good agreement between the estimated and computed heights (Figures 12c and 12d).

[39] The error factor κ is derived from the amplitude ratio, which is the ratio of the estimated tsunami heights to computed amplitudes at a given site. The geometric mean $K$ of the amplitude ratios at all the sites is a measure of the relative size of the actual and modeled sources [e.g., *Aida*, 1978]. The average slip on the assumed fault is calculated such that $K = 1$. Following *Aida* [1978], we further assume that the amplitude ratio obeys a lognormal probability distribution $N$ (log $K$, log κ), where log κ is the standard deviation of random variable log $K$. It follows that parameter κ represents an error factor with respect to $K$; there is 68% probability that $K$ lies within the range of factor κ that is, between $K/\kappa$ and $K\kappa$.

[40] The correlation coefficient $r$ describes agreement between the estimated and computed tsunami amplitudes at all the sites. Perfect agreement would yield $r = 1$.

[41] Both κ and $r$ measure site-specific errors from the estimation of heights in section 2 and from the computation of heights in section 4. Not represented in these statistics are

[1]Auxiliary material is available at ftp://www.agu.org/apend/jb/2003JB002521.

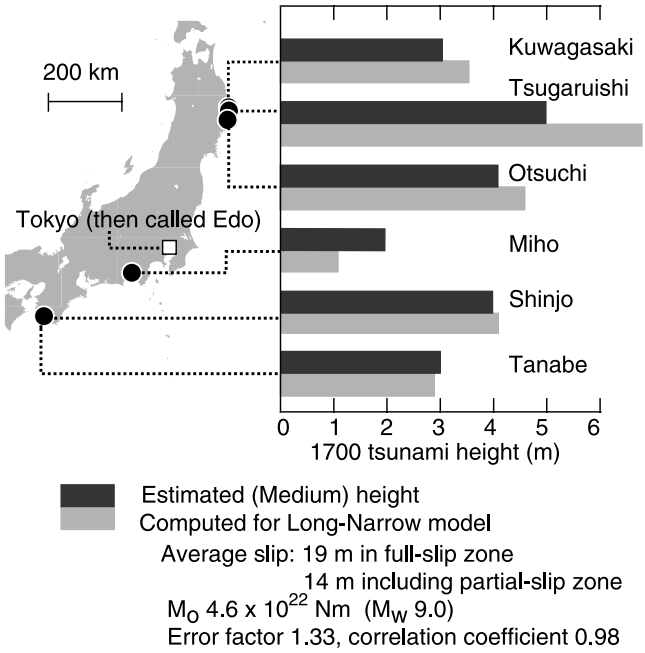


**Figure 11.** Comparison of the tsunami heights along Japan's Pacific coast based on descriptions of damage and flooding (medium height set; Tables 3a–3c) and as computed from seafloor displacement at Cascadia (Long-Narrow model).

systematic errors in height estimation and tsunami computation that affect all sites equally.

### 5.2. Comparison of Tsunami Heights

[42] The computed tsunami heights agree most with the estimated heights of the medium set (Figures 12c and 12d and Tables 5a–5c). This agreement is best with a Long-Narrow rupture (Figure 11). Both the medium and the Long-Narrow heights show the resonance in Miyako Bay that made the 1960 Chile tsunami larger at Tsugaruishi than at Kuwagasaki (section 2.2). Resonance probably also explains why the tsunami heights in Figure 11 are larger at Shinjo than the nearby Tanabe, as was the case in the 1960 tsunami (Table 3d). The relatively low height at Miho, again seen in 1960, may result from local or regional bathymetry. The error factor $\kappa$ and the correlation coefficient $r$, 1.33 and 0.98, respectively, imply that the computed tsunami closely simulates variation in medium height among the six sites.

[43] The two other sets of 1700 tsunami height (*Tsuji et al.* [1998] and low sets) show poorer agreement with computed heights (Figures 12c and 12d), much as they also depart from the pattern of heights measured for the 1960 tsunami (Figure 2b). The *Tsuji et al.* [1998] set gives the smallest correlation coefficients. The low set gives the largest error factors.

[44] The measures of agreement, $\kappa$ and $r$, thus vary more among sets of height estimates than they do among rupture models (Figures 12c and 12d). Our slip and moment estimates therefore contain more uncertainty from local

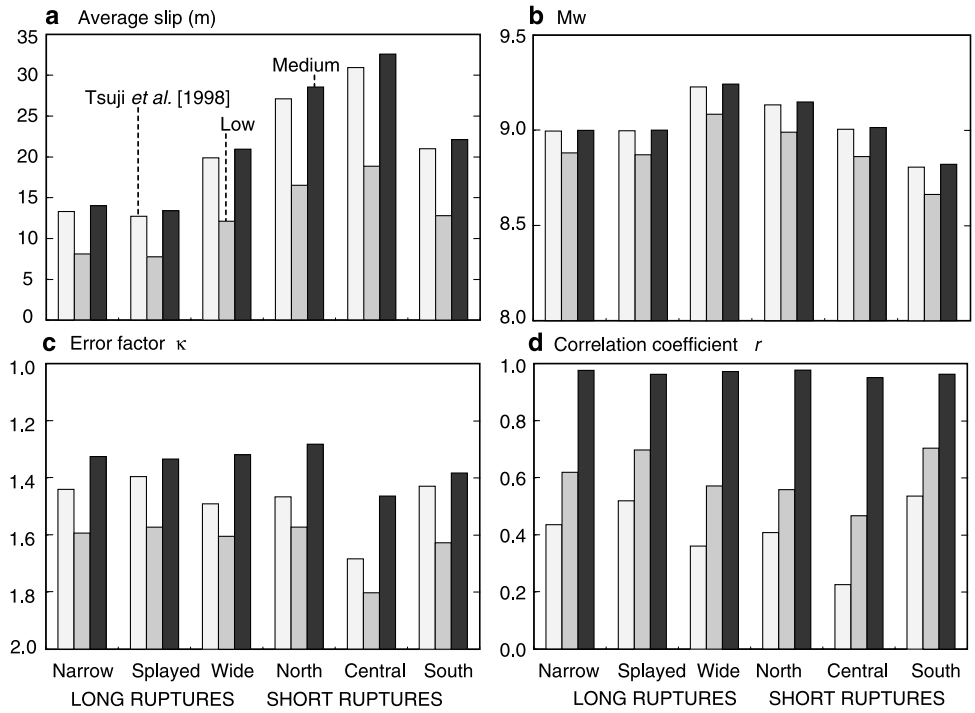


**Figure 12.** Eighteen estimates of (a) seismic slip, (b) moment magnitude $M_w$, (c) error factor $\kappa$, and (d) correlation coefficient $r$, for the six rupture models (Figure 8) and the three sets of tsunami height estimates (Figure 2). The vertical axis for Figure 12c is reversed so that the higher the bars, the better the agreements.

**Table 5a.** Computed Tsunami Heights and Fault Parameters for *Tsuji et al.* [1998] Heights

| | Estimated | Long-Narrow | Long-Splayed | Long-Wide | Short-North | Short-Central | Short-South |
|---|---|---|---|---|---|---|---|
| Average slip, m | | 13 | 13 | 20 | 27 | 31 | 21 |
| Seismic moment, $10^{22}$ N m | | 4.3 | 4.2 | 8.7 | 6.3 | 4.1 | 2.0 |
| Moment magnitude, $M_w$ | | 9.0 | 9.0 | 9.2 | 9.1 | 9.0 | 8.8 |
| Error factor | | 1.44 | 1.40 | 1.49 | 1.47 | 1.68 | 1.43 |
| Correlation coefficient | | 0.44 | 0.52 | 0.36 | 0.41 | 0.23 | 0.54 |
| Tsunami heights, m | | | | | | | |
| Kuwagasaki | 4 | 3.4 | 3.7 | 3.1 | 2.8 | 2.7 | 3.8 |
| Tsugaruishi | 3.2 | 6.4 | 6.1 | 7.0 | 6.9 | 8.3 | 6.0 |
| Otsuchi | 3.3 | 4.3 | 4.1 | 4.3 | 4.0 | 5.2 | 4.6 |
| Nakaminato[a] | 1 | 2.7 | 3.2 | 3.1 | 2.9 | 2.7 | 3.6 |
| Miho | 1.4 | 1.1 | 1.0 | 1.1 | 1.2 | 1.0 | 1.0 |
| Shinjo | 5.4 | 3.9 | 4.0 | 3.9 | 4.3 | 3.7 | 4.2 |
| Tanabe | 3.3 | 2.7 | 2.7 | 2.6 | 2.6 | 2.5 | 2.5 |

[a]Nakaminato was not used for computations of slip, error factor, and correlation coefficient because it lacks description of flooding or damage onshore.

factors in estimating and computing tsunami heights than from variation in rupture models.

### 5.3. Fault Slip and Seismic Moment

[45] The medium height set produces reasonable slip amounts on the fault. Averaged across the full-slip and partial-slip zones, the slip is 13–21 m for the three long-rupture models and 22–33 m for the short rupture models (Figure 12a). The average slip on the full-slip zone alone is 18–21 m for all the long-rupture models and 29–44 m for the three short rupture models (Table 4).

[46] Any of these estimates of slip on the full-slip zone may be consistent with the potential seismic slip that is computed as the product of plate-convergence rate and paleoseismological recurrence intervals. The range 18–21 m for the long-rupture models and medium heights is consistent with convergence at 40 mm/yr [*Wang et al.*, 2003] through an average recurrence interval of about 500 years [*Adams*, 1990; *Atwater and Hemphill-Haley*, 1997; *Kelsey et al.*, 2002]. Larger slip might be explained by an unusually long interseismic interval before the 1700 earthquake. Such an interval has been inferred along the southern Washington coast, where the pre-1700 interval has an estimated length of 600–900 years [*Atwater and Hemphill-Haley*, 1997].

[47] Within each set of estimated tsunami heights, there is little difference among long-rupture models in the amount of coseismic slip. The low heights require the smallest slip averaged across the full-rupture and partial-rupture zones, 8–12 m for the long-rupture models, 13–19 m for the short rupture models. The *Tsuji et al.* [1998] heights increase this average to 13–20 m for the long-rupture models and to 21–31 m for the short rupture models. The medium heights give the largest slip, 13–21 m for long ruptures and 22–33 m for short ruptures (Table 4). Among the short ruptures, the Short-Central model requires the largest slip because its length is the shortest. The Short-North rupture model requires larger slip than Short-South, although the Short-North rupture is longer. This difference may result from the location and orientation (radiation pattern) of the tsunami source; the Short-South model is the most effective among the three short ruptures in terms of tsunami run-up in Japan.

[48] These various estimates of seismic slip imply seismic moment on the order of $10^{22}$ N m. Seismic moment is the product of rupture area, slip, and rigidity. For rigidity, we use $4 \times 10^{10}$ N/m$^2$ (Pa), a typical value at a depth of 20 km [*Dziewonski and Anderson*, 1981]. The results are 1.2–9.2 $\times$ $10^{22}$ N m for the 18 combinations of tsunami heights and rupture models (Table 4). The range for the combinations of medium heights and long-rupture models is 4.4–9.2 $\times$ $10^{22}$ N m or within approximately a factor of 2.

[49] These estimates of seismic moment ($M_0$) correspond to moment magnitudes ($M_w$) close to 9 (Figure 12). Here we use the $M_w$-$M_0$ relationship of *Kanamori* [1977]: $M_w = (\log M_0 - 9.1)/1.5$, where the unit of $M_0$ is N m. The range of moment magnitude is 8.7–9.2 among all the combinations and 9.0–9.2 for the combinations of medium heights and long-rupture models. (A factor of 2 in $M_0$ corresponds to 0.2 in $M_w$.) Uncertainties that these ranges may fail to express are summarized below, in section 8.

[50] The assumption that fault slip at Cascadia varies linearly with tsunami height in Japan (section 4.1) means that a tenfold increase in tsunami height in Japan corre-

**Table 5b.** Computed Tsunami Heights and Fault Parameters for the Low Heights

| | Estimated | Long-Narrow | Long-Splayed | Long-Wide | Short-North | Short-Central | Short-South |
|---|---|---|---|---|---|---|---|
| Average slip, m | | 8 | 8 | 12 | 17 | 19 | 13 |
| Seismic moment, $10^{22}$ N m | | 2.6 | 2.6 | 5.3 | 3.9 | 2.5 | 1.2 |
| Moment magnitude, $M_w$ | | 8.9 | 8.9 | 9.1 | 9.0 | 8.9 | 8.7 |
| Error factor | | 1.59 | 1.57 | 1.60 | 1.57 | 1.80 | 1.63 |
| Correlation coefficient | | 0.62 | 0.70 | 0.57 | 0.56 | 0.47 | 0.70 |
| Tsunami heights, m | | | | | | | |
| Kuwagasaki | 2.4 | 2.0 | 2.2 | 1.9 | 1.7 | 1.6 | 2.3 |
| Tsugaruishi | 2.2 | 3.9 | 3.7 | 4.3 | 4.2 | 5.1 | 3.6 |
| Otsuchi | 1.9 | 2.6 | 2.5 | 2.6 | 2.4 | 3.2 | 2.8 |
| Miho | 1.6 | 0.6 | 0.6 | 0.7 | 0.7 | 0.6 | 0.6 |
| Shinjo | 2.1 | 2.4 | 2.5 | 2.4 | 2.6 | 2.2 | 2.5 |
| Tanabe | 1.6 | 1.7 | 1.7 | 1.6 | 1.6 | 1.5 | 1.5 |

**Table 5c.** Computed Tsunami Heights and Fault Parameters for the Medium Heights

| | Estimated | Long-Narrow | Long-Splayed | Long-Wide | Short-North | Short-Central | Short-South |
|---|---|---|---|---|---|---|---|
| Average slip, m | | 14 | 13 | 21 | 29 | 33 | 22 |
| Seismic moment, $10^{22}$ N m | | 4.6 | 4.4 | 9.2 | 6.7 | 4.3 | 2.1 |
| Moment magnitude, $M_w$ | | 9.0 | 9.0 | 9.2 | 9.1 | 9.0 | 8.8 |
| Error factor | | 1.33 | 1.33 | 1.32 | 1.28 | 1.46 | 1.38 |
| Correlation coefficient | | 0.98 | 0.96 | 0.97 | 0.98 | 0.95 | 0.96 |
| Tsunami heights, m | | | | | | | |
| Kuwagasaki | 3 | 3.5 | 3.9 | 3.2 | 3.0 | 2.8 | 4.0 |
| Tsugaruishi | 5 | 6.8 | 6.4 | 7.4 | 7.3 | 8.8 | 6.3 |
| Otsuchi | 4 | 4.5 | 4.3 | 4.5 | 4.2 | 5.5 | 4.8 |
| Miho | 2 | 1.1 | 1.1 | 1.2 | 1.3 | 1.0 | 1.0 |
| Shinjo | 4 | 4.1 | 4.3 | 4.1 | 4.6 | 3.9 | 4.4 |
| Tanabe | 3 | 2.9 | 2.9 | 2.7 | 2.7 | 2.7 | 2.7 |

sponds, at Cascadia, to a tenfold increase in seismic slip, a tenfold increase in seismic moment, and a 0.67-unit increase in moment magnitude $M_w$. However, in the tsunami magnitude formulas of *Abe* [1979, 1989], a tenfold increase in distant tsunami height corresponds to a one-unit increase in tsunami magnitude $M_t$, which has been calibrated to be equivalent to $M_w$. Stated conversely, distant tsunami height appears to increase 32-fold with each unit of $M_w$ in our scaling, while in Abe's it increases only about tenfold. The difference results from our assumption that rupture width and length are fixed. If these also increase with seismic slip, they should add to the seismic moment.

## 6. Which Rupture Models Agree With Paleoseismological Evidence at Cascadia?

[51] Among the six rupture models with which we computed these earthquake parameters, only long ruptures, with slip of about 20 m in the full-slip zone, appear consistent with the pattern and estimated amounts of coastal coseismic subsidence at Cascadia. Shorter ruptures with larger slips appear at odds with paleoseismological evidence: the Short-North and Short-Central models predict more subsidence than what occurred around 1700, while Short-South predicts no change in land level where land subsided in 1699–1700.

[52] To make these comparisons, we plot three categories of paleoseismological sites on contour maps of predicted coseismic vertical displacement (Figure 8): (1) five sites where amounts of coseismic subsidence have been estimated from statistical comparisons between modern and fossil assemblages of microscopic fossils [*Hemphill-Haley*, 1995; *Nelson et al.*, 1996, 1998; *Shennan et al.*, 1996, 1998; *Guilbault et al.*, 1996; *Hughes et al.*, 2002]; (2) four sites where subsidence-induced death of trees has been dated to the months between August 1699 and May 1700 [*Yamaguchi et al.*, 1997; *Jacoby et al.*, 1997]; and (3) estuaries where land probably subsided during the 1700 earthquake, but where the amount and timing of that subsidence have not been defined as closely as in categories (1) and (2) [*Peterson et al.*, 1997; *Kelsey et al.*, 1998]. We highlight categories (1) and (2) because they test the model predictions more conclusively than does category (3).

[53] The Long-Narrow and Long-Splayed models predict coseismic subsidence everywhere that coseismic subsidence has been inferred at Pacific coast estuaries of the Cascadia subduction zone (Figures 1 and 8). The predictions also appear consistent with estimated amounts of coseismic subsidence along the Pacific coast (Figures 8a and 8b). This agreement is preliminary without data on coseismic subsidence farther inland, at Puget Sound (Figure 7).

[54] The Long-Wide model predicts uplift near Copalis, Washington (Figure 8c), where land subsided into tidal water about 300 years ago [*Atwater*, 1992] and the death of a submerged tree has been dated to the months between August 1699 and May 1700 [*Yamaguchi et al.*, 1997; *Jacoby et al.*, 1997]. Long-Wide also predicts 2–3 m of subsidence at Netarts Bay, Oregon, where subsidence in 1700 probably did not exceed 1 m [*Shennan et al.*, 1998].

[55] The Short-North and Short-Central models predict about 3 m of subsidence not only at Netarts Bay but also at Grays Harbor, Washington, where the subsidence estimate for the most recent great earthquake is 0.5–1.5 m [*Shennan et al.*, 1996]. The Short-North model further predicts about 3 m of subsidence at Tofino, British Columbia (Figure 8f). Independent paleoecological estimates for the coseismic subsidence at Tofino, one based on foraminifera and the other on pollen, instead imply amounts between about 0.5 and 1.0 m [*Guilbault et al.*, 1996; *Hughes et al.*, 2002].

## 7. Did Submarine Landslides at Cascadia Enlarge the 1700 Tsunami in Japan?

[56] Tectonic seafloor displacement at Cascadia probably accounts for most or all the height of the 1700 tsunami in Japan. Even if landslides at Cascadia enlarged the tsunami, they probably did not enlarge it enough to invalidate our estimates of coseismic slip and seismic moment.

[57] Earthquakes often trigger landslides, both subaerial and submarine, that become secondary sources of tsunamis, especially on nearby coasts. The horizontal scale of such secondary sources is usually much smaller than tectonic seafloor displacement that accompanies earthquake fault motion. Consequently, a landslide's effects on tsunami height are mostly limited to nearby shores. For example, the largest "tsunami" height, more than 500 m at Lituya Bay, Alaska, represents a slosh from an earthquake-induced subaerial rockslide that barely disturbed areas outside the bay [*Lander*, 1996]. The 1964 Alaskan earthquake ($M_w$ 9.2) triggered landslides that became sources of locally large tsunami damage, including Valdez Inlet with more than 60 m run-up [*Coulter and Migliaccio*, 1966]. However, it was

coseismic tectonic displacement in 1964 that generated the trans-Pacific tsunami recorded in Hawaii and Japan [*Johnson et al.*, 1996]. The tsunami from the 1998 Papua New Guinea earthquake ($M_w$ 7.0) reached a near-source height of 15 m without exceeding 5-m high outside a 40 km stretch of coast [*Kawata et al.*, 1999]. A submarine landslide off Papua New Guinea probably accounts for this focused height distribution, while the tsunami's distant height in Japan, ~10 cm or less, is better explained by tectonic displacement of the seafloor [*Tanioka*, 1999].

[58] To produce meters of tsunami height in Japan, landslides at Cascadia would need to displace as much seawater as does seafloor displacement in our models (Figure 8). Such slides would be many times larger than those at Lituya Bay, Valdez, or Papua New Guinea. The seafloor at Cascadia has three submarine landslides with a total area of 8000 km$^2$ (Figure 1). However, these probably formed over 100,000 years ago [*Goldfinger et al.*, 2000].

## 8. Remaining Uncertainties

[59] The 1700 earthquake may have been outside the range of moment magnitudes estimated in section 5.3. We state this possibility because our range of $M_w$ 8.7–9.2 excludes several uncertainties that we found difficult to quantify.

[60] By using several sets of estimated heights, we tried to convey uncertainties in estimating Japanese tsunami heights from historical descriptions of damage and flooding (section 2). Though the ranges of height estimates in Table 2 include all values we found plausible, we cannot rule out heights outside these ranges.

[61] Our elastic dislocation model, with its simple, parallel bands of full slip and partial slip, may oversimplify actual slip on the fault (section 3), although slip heterogeneities would have little effects on distant tsunami heights. The computations of tsunami height may contain systematic errors, common to all sites, from nonlinear effects and from treating each estimated height as comparable to the mean height computed within a cell of a 12″ nearshore grid (section 4.3). The assumed rigidity may be different from the value $4 \times 10^{10}$ N/m$^2$ (Pa) assumed in section 5.3.

## 9. Conclusions

[62] These problems notwithstanding, the 1700 Cascadia earthquake was probably close to $M_w$ 9.0. Eighteen comparisons, three sets of estimated tsunami heights compared with computed tsunami heights from six sets of rupture models, yield $M_0$ in the range $1–9 \times 10^{22}$ N m or $M_w$ 8.7–9.2. The best agreement comes from models with ruptures 1100 km long and average slips of 19 m (within the full-slip zone) and 14 m (average over full-slip and partial-slip zones). For these models, $M_0$ is $5 \times 10^{22}$ N m and $M_w$ 9.0. Shorter rupture models mostly require slip much greater than 20 m, and they would generate coastal land-level changes inconsistent with paleoseismological evidence at Cascadia. Although these conclusions exclude several sources of uncertainty, they strengthen the case that the Cascadia subduction zone is capable of producing earthquakes of $M_w$ 9.

[63] **Acknowledgments.** Yoshinobu Tsuji and Kazue Ueda helped us interpret descriptions of the 1700 tsunami in Japan. Tom Brocher, John Clague, Eric Geist, Alan Nelson, Harvey Kelsey, and Roy Hyndman provided manuscript reviews. Authors' main responsibilities: K. Satake, sections 2, 4, 5, and 7; K. Wang, section 3; B. Atwater, sections 2 and 6. The work represents collaboration between the Geological Surveys of Japan, Canada, and the United States. B. Atwater spent months in Japan with partial support by the Japanese government. Contribution 2002157 of the Geological Survey of Canada.

## References

Abe, K., Size of great earthquakes of 1837–1974 inferred from tsunami data, *J. Geophys. Res.*, *84*, 1561–1568, 1979.

Abe, K., Estimate of tsunami heights from magnitudes of earthquake and tsunami (in Japanese with English abstract), *Bull. Earthquake Res. Inst. Univ. Tokyo*, *64*, 51–69, 1989.

Adams, J., Paleoseismicity of the Cascadia subduction zone: Evidence from turbidites off the Oregon-Washington margin, *Tectonics*, *9*, 569–583, 1990.

Aida, I., Reliability of a tsunami source model derived from fault parameters, *J. Phys. Earth*, *26*, 57–73, 1978.

Atwater, B. F., Geologic evidence for earthquakes during the past 2000 years along the Copalis River, southern coastal Washington, *J. Geophys. Res.*, *97*, 1901–1919, 1992.

Atwater, B. F., and E. Hemphill-Haley, Recurrence intervals for great earthquakes of the past 3,500 years at northeastern Willapa Bay, Washington, *U.S. Geol. Surv. Prof. Pap. 1576*, 108 pp., 1997.

Ben-Menahem, A., and M. Rosenman, Amplitude patterns of tsunami waves from submarine earthquakes, *J. Geophys. Res.*, *77*, 2097–3128, 1972.

Clague, J. J., Evidence for large earthquakes at the Cascadia subduction zone, *Rev. Geophys.*, *35*, 439–460, 1997.

Committee for Field Investigation of the Chilean Tsunami of 1960, *Report on the Chilean Tsunami of May 24, 1960, as Observed Along the Coast of Japan*, 397 pp., Univ. of Tokyo, Tokyo, 1961.

Coulter, H. W., and R. R. Migliaccio, Effects of the earthquake of March 27, 1964 at Valdez, Alaska, *U.S. Geol. Surv. Prof. Pap. 542-C*, 36 pp., 1966.

DeMets, C., and T. H. Dixon, New kinematic models for Pacific-North America motion from 3 Ma to present, 1, Evidence for steady motion and biases in the NUVEL-1A model, *Geophys. Res. Lett.*, *26*, 1921–1924, 1999.

Dziewonski, A. M., and D. L. Anderson, Preliminary reference Earth model, *Phys. Earth Planet. Inter.*, *25*, 297–356, 1981.

Flück, P., R. D. Hyndman, and K. Wang, Three-dimensional dislocation model for great earthquakes of the Cascadia subduction zone, *J. Geophys. Res.*, *102*, 20,539–20,550, 1997.

Frankel, A. D., et al., USGS national seismic hazard maps, *Earthquake Spectra*, *16*, 1–19, 2000.

Geist, E., and R. Dmowska, Local tsunamis and distributed slip at the source, *Pure Appl. Geophys.*, *154*, 485–512, 1999.

Goldfinger, C., L. D. Kulm, L. C. McNeill, and P. Watts, Super-scale failure of the southern Oregon Cascadia margin, *Pure Appl. Geophys.*, *157*, 1189–1226, 2000.

Guilbault, J.-P., J. J. Clague, and M. Lapointe, Foraminiferal evidence for the amount of coseismic subsidence during a late Holocene earthquake on Vancouver Island, west coast of Canada, *Quat. Sci. Rev.*, *15*, 913–937, 1996.

Heaton, T. H., and H. Kanamori, Seismic potential associated with subduction in the northwestern United States, *Bull. Seismol. Soc. Am.*, *74*, 933–941, 1984.

Hemphill-Haley, E., Diatom evidence for earthquake-induced subsidence and tsunami 300 yr ago in southern coastal Washington, *Geol. Soc. Am. Bull.*, *107*, 367–378, 1995.

Hughes, J. F., R. W. Mathewes, and J. J. Clague, Use of pollen and vascular plants to estimate coseismic subsidence at a tidal marsh near Tofino, British Columbia, *Palaeogeogr. Palaeoclimatol. Palaeoecol.*, *185*, 145–161, 2002.

Hyndman, R. D., and K. Wang, The rupture zone of Cascadia great earthquakes from current deformation and thermal regime, *J. Geophys. Res.*, *100*, 22,133–22,154, 1995.

Jacoby, G. C., D. E. Bunker, and B. E. Benson, Tree-ring evidence for an AD 1700 Cascadia earthquake in Washington and northern Oregon, *Geology*, *25*, 999–1002, 1997.

Johnson, J. M., K. Satake, S. R. Holdahl, and J. Sauber, The 1964 Prince William Sound earthquake: Joint inversion of tsunami and geodetic data, *J. Geophys. Res.*, *101*, 523–532, 1996.

Kanamori, H., The energy release in great earthquakes, *J. Geophys. Res.*, *82*, 2981–2987, 1977.

Kato, Y., Z. Suzuki, K. Nakamura, A. Takagi, K. Emura, M. Ito, and H. Ishida, The Chile tsunami of May 24, 1960 observed along the Sanriku coast, Japan, in *Report on the Chilean Tsunami of May 24, 1960, as Observed Along the Coast of Japan*, pp. 67–76, Univ. of Tokyo, Tokyo, 1961.

Kawata, Y., B. C. Benson, J. C. Borrero, J. L. Borrero, H. L. Davies, W. P. de Lange, F. Imamura, H. Lets, J. Nott, and C. E. Synolakis, Tsunami in Papua New Guinea was as intense as first thought, *Eos Trans. AGU*, *80*, 101, 105, 1999.

Kelsey, H. M., R. C. Witter, and E. Hemphill-Haley, Response of a small Oregon estuary to coseismic subsidence and postseismic uplift in the past 300 years, *Geology*, 231–234, 1998.

Kelsey, H. M., R. C. Witter, and E. Hemphill-Haley, Plate-boundary earthquakes and tsunamis of the past 5500 yr, Sixes River estuary, southern Oregon, *Geol. Soc. Am. Bull.*, *114*, 298–314, 2002.

Kon'no, E., (Ed.), Geological observations of the Sanriku coastal region damaged by tsunami due to the Chile earthquake in 1960, *Contrib. Inst. Geol. Paleontol. Tohoku Univ.*, *52*, 1–40, 1961.

Lander, J., Tsunamis affecting Alaska 1737–1996, *Geophys. Res. Doc. 31*, 195 pp., Natl. Geophys. Data Cent., Boulder, Colo., 1996.

McCaffrey, R., M. D. Long, C. Goldfinger, P. C. Zwick, J. L. Nabelek, C. K. Johnson, and C. Smith, Rotation and plate locking along the southern Cascadia subduction zone, *Geophys. Res. Lett.*, *27*, 3117–3120, 2000.

Miller, M. M., D. J. Johnson, C. M. Rubin, H. Dragert, K. Wang, A. Qamar, and C. Goldfinger, GPS-determination of along-strike variation in Cascadia margin kinematics: Implications for relative plate motion, subduction zone coupling, and permanent deformation, *Tectonics*, *20*, 161–176, 2001.

Nelson, A. R., et al., Radiocarbon evidence for extensive plate-boundary rupture about 300 years ago at the Cascadia subduction zone, *Nature*, *378*, 371–374, 1995.

Nelson, A. R., A. E. Jennings, and K. Kashima, An earthquake history derived from stratigraphic and microfossil evidence of relative sea-level change at Coos Bay, southern coastal Oregon, *Geol. Soc. Am. Bull.*, *108*, 141–154, 1996.

Nelson, A. R., Y. Ota, M. Umitsu, K. Kashima, and Y. Matsushima, Seismic or hydrodynamic control of rapid late-Holocene sea-level rises in southern coastal Oregon, USA?, *Holocene*, *8*, 287–299, 1998.

Peterson, C. D., E. T. Barnett, G. G. Briggs, G. A. Carver, J. J. Clague, and M. E. Darienzo, Estimates of coastal subsidence from great earthquakes in the Cascadia subduction zone, Vancouver B. C. Island, Washington, Oregon, and northernmost California, *Oreg. State Dep. Geol. Miner. Ind. Open File Rep., O-97-5*, 44 pp., 1997.

Petersen, M. D., C. H. Cramer, and A. D. Frankel, Simulations of seismic hazard for the Pacific Northwest of the United States from earthquakes associated with the Cascadia subduction zone, *Pure Appl. Geophys.*, *159*, 2147–2168, 2002.

Priest, G. R., E. Myers, A. M. Baptista, P. Flueck, K. Wang, and C. D. Peterson, Source simulation for tsunamis: Lessons learned from fault rupture modeling of the Cascadia subduction zone, *Sci. Tsunami Hazards*, *18*, 77–106, 2000.

Satake, K., Tsunamis, in *International Handbook of Earthquake and Engineering Seismology*, Part A, edited by W. H. K. Lee et al., pp. 437–451, Academic, San Diego, Calif., 2002.

Satake, K., K. Shimazaki, Y. Tsuji, and K. Ueda, Time and size of a giant earthquake in Cascadia inferred from Japanese tsunami records of January 1700, *Nature*, *379*, 246–249, 1996.

Savage, J. C., M. Lisowski, and W. H. Prescott, Geodetic strain measurements in Washington, *J. Geophys. Res.*, *86*, 4929–4940, 1981.

Savage, J. C., J. L. Svarc, W. H. Prescott, and M. H. Murray, Deformation across the forearc of the Cascadia subduction zone at Cape Blanco, Oregon, *J. Geophys. Res.*, *105*, 3095–3120, 2000.

Shennan, I., A. J. Long, M. M. Rutherford, F. M. Green, J. B. Innes, J. M. Lloyd, Y. Zong, and K. J. Walker, Tidal marsh stratigraphy, sea-level change and large earthquakes, I, A 5000 year record in Washington, U.S.A., *Quat. Sci. Rev.*, *15*, 1023–1059, 1996.

Shennan, I., A. J. Long, M. M. Rutherford, J. B. Innes, F. M. Green, and K. J. Walker, Tidal marsh stratigraphy, sea-level change and large earthquakes, II, Submergence events during the last 3500 years at Netarts Bay, Oregon, U.S.A., *Quat. Sci. Rev.*, *17*, 365–393, 1998.

Tanioka, Y., Analysis of the far-field tsunamis generated by the 1998 Papua New Guinea earthquake, *Geophys. Res. Lett.*, *26*, 3393–3396, 1999.

Tsuji, Y., K. Ueda, and K. Satake, Japanese tsunami records from the January 1700 earthquake in the Cascadia subduction zone (in Japanese with English abstract), *J. Seismol. Soc. Jpn.*, *51*, 1–17, 1998.

Wang, K., Simplified analysis of horizontal stresses in a buttressed forearc sliver at an oblique subduction zone, *Geophys. Res. Lett.*, *23*, 2021–2024, 1996.

Wang, K., J. He, H. Dragert, and T. James, Three-dimensional viscoelastic interseismic deformation model for the Cascadia subduction zone, *Earth Planets Space*, *53*, 295–306, 2001.

Wang, K., R. Wells, S. Mazzotti, R. D. Hyndman, and T. Sagiya, A revised dislocation model of interseismic deformation of the Cascadia subduction zone, *J. Geophys. Res.*, *108*(B1), 2026, doi:10.1029/2001JB001227, 2003.

Watanabe, H., *Comprehensive List of Tsunamis to Hit the Japanese Islands* (in Japanese), 2nd ed., 238 pp., Univ. of Tokyo Press, Tokyo, 1998.

Wells, R. E., and R. W. Simpson, Northward migration of the Cascadia forearc in the northwestern U.S. and implications for subduction deformation, *Earth Planets Space*, *53*, 275–283, 2001.

Wells, R. E., C. S. Weaver, and R. J. Blakely, Forearc migration in Cascadia and its neotectonic significance, *Geology*, *26*, 759–762, 1998.

Wells, R. E., R. J. Blakely, Y. Sugiyama, D. W. Scholl, and P. A. Dinterman, Basin-centered asperities in great subduction zone earthquakes: A link between slip, subsidence and subduction erosion?, *J. Geophys. Res.*, *108*(B10), 2507, doi:10.1029/2002JB002072, 2003.

Yamaguchi, D. F., B. F. Atwater, D. E. Bunker, B. E. Benson, and M. S. Reid, Tree-ring dating the 1700 Cascadia earthquake, *Nature*, *389*, 922–923, 1997.

B. F. Atwater, United States Geological Survey at Department of Earth and Space Sciences, University of Washington, Seattle, WA 98195-1310, USA. (atwater@u.washington.edu)

K. Satake, Active Fault Research Center, National Institute of Advanced Industrial Science and Technology (GSJ/AIST), Site C7 1-1-1 Higashi, Tsukuba 305-8567, Japan. (kenji.satake@aist.go.jp)

K. Wang, Pacific Geoscience Centre, Geological Survey of Canada, Sidney, British Columbia, Canada V8L 4B2. (wang@pgc.nrcan.gc.ca)